Analytic I_{sc}–V_{oc} Method and Power Loss Modes From Outdoor Time-Series I–V Curves

Menghong Wang, Jiqi Liu, Tyler J. Burleyson, Eric J. Schneller, Kristopher O. Davis, Roger H. French, *Member, IEEE*, and Jennifer L. Braid, *Member, IEEE*

***Abstract*—Utilizing large-scale outdoor I–V data streams, the authors demonstrated a feasible, repeatable method to construct outdoor time-series I_{sc}–V_{oc} curves. Resulting *Analytic* I_{sc}–V_{oc} curves are validated with laboratory $Suns$-V_{oc} measurements. Comparing I_{sc}–V_{oc} with real I–V curves, power loss modes including uniform current loss, recombination loss, series resistance loss, and current mismatch loss can be quantified in units of watts or percent nominal power, making them directly comparable. Above power loss modes are calculated for long-term I–V data from fielded modules in different climate zones, and dominant power loss modes were determined from the resulting time series. This method has been published as an open source package in R programming language.**

***Index Terms*—Data-driven, data-mining, degradation, in situ I–V, power loss, $Suns$-V_{oc}, time series.**

I. Introduction

BEING a reliable source of renewable energy, the size of global installed photovoltaic energy capacity continues growing rapidly, with almost 100 GW of PV modules installed in 2018 and 592 TWh of PV electricity produced in 2018 [1]. The long term reliability of PV modules used in real world environments is a critical area of research, since it plays an important role in determining the performance over lifetime and the resulting levelized cost of electricity (LCOE) [2]. There have been numerous discussions about analyzing the maximum power of solar modules both under outdoor exposure and indoor accelerated tests [3]–[8]. Aside from the reduction of maximum power, which is a well-known sign of degradation of PV modules, I–V features of PV modules can also convey important mechanistic insights into causes of power degradation [9], [10]. Acquisition of I–V data in the field is an opportunity to better understand real-world module performance [11],[12]. However, there are numerous possible degradation modes for an outdoor PV system, and these modes are not uniquely associated with commonly extracted I–V characteristics such as short circuit current (I_{sc}), open circuit voltage (V_{oc}), series resistance (R_s), shunt resistance (R_{sh}), and fill factor (FF). Furthermore, the relative changes in I–V characteristics may not reflect their effects on the power output of the module, i.e., the changes in I–V characteristics are not directly comparable.

Alternatively, $Suns$-V_{oc} can be used to obtain more detailed information about the PV module's performance and specific degradation modes [13]–[15].

$Suns$-V_{oc} is a common characterization technique for both cells and modules that can be performed either by transient or quasistatic illumination [16]. Comparison of I–V and $Suns$-V_{oc} curves is useful for quantifying nonuniform module degradation or power loss modes, such as current mismatch, physical damage, and cell shunting, which cannot be identified from standard I–V parameters.

While the $Suns$-V_{oc} curve is usually constructed from indoor experimental measurement data, it can also be extracted from outdoor data [13], [17]. A similar method, $Suns$-V_{mp}, has also been proposed by Sun *et al.* [18], which takes the maximum power point instead of I_{sc}–V_{oc} pairs to obtain a pseudo I–V curve. Here, we propose a new dimension-reduction technique called *Analytic* I_{sc}–V_{oc} for more specific determination of power loss mechanisms from time-series I–V parameters extracted from real-world outdoor data.

Unlike indoor measurements, outdoor I–V curves are collected under various irradiance levels and temperatures. Most I–V features have clear irradiance and temperature dependences, as can be seen in Sandia's Photovoltaic Array Performance model [19]. For example, the physical model of V_{oc} is given by

$$V_{oc} = V_{oc0} + N_C \cdot \delta(T_c)\ln(E_e) + \beta_{V_{oc}}(T_c - T_0) \quad (1)$$

where

$$\delta(T_c) = n \cdot k_B \cdot (T_c + 273.15)/q \quad (2)$$

$$E_e = \frac{I_{sc}}{I_{sc0} \cdot (1 + \alpha_{I_{sc}} \cdot (T_c - T_0))}. \quad (3)$$

Manuscript received March 18, 2020; accepted April 28, 2020. This work was supported by the U.S. Department of Energy's Office of Energy Efficiency and Renewable Energy under Solar Energy Technologies Office Agreement Number DE-EE0008172. The work of Jennifer L. Braid was supported by the U.S. Department of Energy (DOE) Office of Energy Efficiency and Renewable Energy administered by the Oak Ridge Institute for Science and Education (ORISE) for the DOE. ORISE is managed by Oak Ridge Associated Universities under DOE contract number DE-SC0014664. *(Corresponding author: Jennifer L. Braid.)*

Menghong Wang is with SDLE Research Center, Case Western Reserve University, Cleveland, OH 44106 USA, and also with the Department of Macromolecular Science and Engineering, Case Western Reserve University, Cleveland, OH 44106 USA (e-mail: mxw477@case.edu).

Tyler J. Burleyson is with SDLE Research Center, Case Western Reserve University, Cleveland, OH 44106 USA (e-mail: tjb152@case.edu).

Eric J. Schneller and Kristopher O. Davis are with the Materials Science and Engineering, University of Central Florida, Orlando, FL 32816 USA (e-mail: eschneller@knights.ucf.edu; kristopher.davis@ucf.edu).

Jiqi Liu, Roger H. French, and Jennifer L. Braid are with SDLE Research Center, Case Western Reserve University, Cleveland, OH 44106 USA, and also with the Department of Materials Science and Engineering, Case Western Reserve University, Cleveland, OH 44106 USA (e-mail: jxl1763@case.edu; roger.french@case.edu; jlb269@case.edu).

Color versions of one or more of the figures in this article are available online at https://ieeexplore.ieee.org.

Digital Object Identifier 10.1109/JPHOTOV.2020.2993100

Here, subscript 0 indicates reference condition (RC), N_c is the number of cells in series, T_c is the cell temperature, $\delta(T_c)$ is the "thermal voltage" defined by (2), and E_e is the effective solar irradiance defined by (3). $\beta_{V_{oc}}$ and $\alpha_{I_{sc}}$ are temperature coefficients for V_{oc} and I_{sc}, respectively, n is the ideality factor, k_B is Boltzmann's constant, and q is an elementary charge. This equation indicates that V_{oc} is linear with the natural logarithm of irradiance.

The modeling of current and voltage at maximum power (I_{mp} and V_{mp}), as a comparison, relies on more empirical parameters

$$I_{mp} = I_{mp0} \cdot \{C_0 \cdot E_e + C_1 \cdot E_e^2\} \cdot \{1 + \alpha_{I_{mp}}(T_c - T_0)\} \quad (4)$$

$$V_{mp} = V_{mp0} + C_2 N_C \cdot \delta(T_c)\ln(E_e) + C_3 N_c \{\delta(T_c)\ln(E_e)\}^2 + \beta_{V_{mp}}(E_e)(T_c - T_0) \quad (5)$$

where C_i ($i = 0, 1, 2, 3$) are empirical constants.

Then, the maximum power (P_{mp}) is simply

$$P_{mp} = I_{mp} \cdot V_{mp}. \quad (6)$$

Modeling of R_s, on the other hand, can be more complicated. According to Wang *et al.* [20], based on single-diode model, the dynamic series resistance R_s of a module can be expressed as

$$R_s = R_{s0} - \frac{N_c}{I_{sc}} \frac{nk_B(T_c + 273.15)}{q} \quad (7)$$

where R_{s0} is the series resistance at open circuit condition.

With the above physics-based models, the V_{oc} values collected at various temperatures from real-world, outdoor I–V curves can be corrected to the same reference temperature. Together with I_{sc} values collected under varying irradiances, the I_{sc}–V_{oc} curve can be constructed.

Using the method specified in previous work [13], [21], [22] to compare I_{sc}–V_{oc} and I–V curves, several power loss modes can also be generated as time series for degradation rate analysis. I–V features including I_{mp}, V_{mp}, and R_s can also be corrected to the same irradiance and temperature, to allow for power loss modes calculation.

II. *Analytic* I_{sc}–V_{oc} Method

The process of constructing outdoor I_{sc}–V_{oc} curves, and preparing I_{sc}–V_{oc} and I–V curves for power loss mode calculations is given in Fig. 1.

A. Data Prerequisites and RC

Similar to the laboratory-based $Suns$-V_{oc} measurement which controls the illumination level to obtain varying I_{sc} and V_{oc} pairs, the naturally varying solar irradiance enables construction of outdoor I_{sc}–V_{oc}. In order to perform a temperature correction of the I–V characteristics, the module temperature (T_m) is required, which can be measured by a thermocouple attached to the module backsheet. In addition, the plane of array irradiance (POA) G_{POA} is used to determine the I_{sc} value at 1 sun, as well as performing irradiance correction for I–V features including I_{mp}, V_{mp}, and R_s. It is preferred to have a pyranometer installed on the fixed rack or tracker, on the same plane of the module. Although it is possible to convert

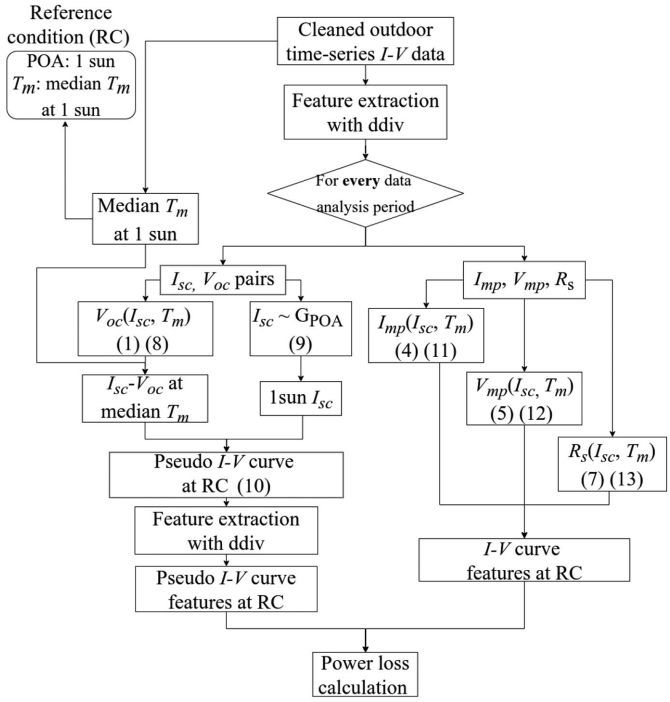

Fig. 1. Demonstration of the process of obtaining outdoor I_{sc}–V_{oc} curve and preparation for power loss calculation. Corresponding equation numbers for each of the process are included here.

global horizontal irradiance (GHI) to G_{POA}, it relies on not only geographic parameters, but also other factors such as ground reflection and sky diffusion. This will bring a lot more variability to the estimated G_{POA}, especially for a tracker system. For the simplicity of analysis, other weather data such as wind speed and air mass are not used in this method.

To ensure better modeling accuracy, a shorter time interval between the I–V curves is preferred. The data analysis period, i.e., how many days of data are used to construct an outdoor I_{sc}–V_{oc} curve, is selected based on the time interval or frequency of I–V curves. For example, for the Fraunhofer-ISE dataset used in this work, one I_{sc}–V_{oc} curve is constructed from a 7-day data analysis period. With I–V curves recorded every 5 min and approximately 8 h of daylight daily, that results in 600 data points being used to build one *Analytic* I_{sc}–V_{oc} curve.

Once the data analysis period has been chosen, predictive models of the I–V features, including I_{sc}, V_{oc}, I_{mp}, V_{mp}, and R_s, are built for each period, capturing characteristics of the module at each specific time. Then, V_{oc} values under various irradiances will be corrected to reference temperature, and paired with corresponding raw I_{sc} values, the I_{sc}–V_{oc} curve can be constructed. Then, I–V features for mechanistic power loss calculations, including I_{mp}, V_{mp}, and R_s, are corrected to the reference temperature and irradiance.

Although standard test conditions (STC) are used in indoor $Suns$-V_{oc} test, it is unrealistic to have a module temperature of 25 °C at 1 sun irradiance (1000 W/m^2). Thus, in the current work, the corrected module temperature T_m^{RC} for outdoor $Suns$-V_{oc} curves is determined based on the real operating temperature

TABLE I
I–V TRACER RANGE AND CORRESPONDING ACCURACY

I-V tracer	Range (V/I)	Accuracy
ET Instrument ESL Solar 500	100V/10A	0.2%
Daystar MT5 multi-tracer	100V/10A	0.1% ± 0.02%

range of each specific module. Taking the data of a single module with G_{POA} between 995 and 1005 W/m^2, the median module temperature T_m of these curves will be T_m^{RC}. Then, the RC used in current work is selected to be 1 sun irradiance ($G_{\text{POA}} = 1000$ W/m^2) or corresponding I_{sc} at 1 sun ($I_{\text{sc}}^{\text{RC}}$), and T_m^{RC} unique to each module.

While some methods of solar module degradation analysis focus on the behavior of P_{mp} at high irradiance, here, we want to avoid intensive filtering of the data for this *Analytic* I_{sc}–V_{oc} analysis so as to retain as much information from the dataset as possible.

For example, a common irradiance cutoff point of recorded I–V curves for some power plants is set to be 100 W/m^2, which has a corresponding I_{sc} of roughly 1 A. Although it seems to be a small value compares to the I_{sc} at 1 sun, removing I_{sc} below 1 A will result in losing nearly half of the I_{sc}–V_{oc} curve, including the pseudo maximum power point. Another type of common filtering is to remove all "abnormal" data such as snow days or even nonclearsky days. While this operation will make analysis of P_{mp}-based degradation rate calculation easier, it would also remove some of the power loss modes that we would want to capture with current method.

Therefore, all I–V curves with I_{sc} greater that the tracer's accuracy level are used in the analysis, and no other filtering was done based on the assumed validity of I–V curve.

The accuracies of the two I–V tracers used in this article are listed in Table I. For curves recorded by the ESL Solar 500 device, only data with I_{sc} larger than 0.02 A and V_{oc} above 0.2 V should be used.

B. Constructing I_{sc}–V_{oc} Curve

In indoor experimental conditions, the illumination is controlled and I_{sc} changes monotonically with little to no variation in module temperature. However, for real-world data, it is necessary to correct the V_{oc} values taken at different irradiances to a single uniform temperature.

Considering that cell temperature T_c is usually not available in real life applications of solar modules, module temperature T_m can be used as an approximation in (1). If we assume that $\alpha_{I_{\text{sc}}}$ is negligible, then the effective solar irradiance E_e given in (3) is equivalent to I_{sc}/Const. Thus, (1) can be simplified to

$$V_{\text{oc}}(I_{\text{sc}}, T_m) = \alpha_0 + \alpha_1 \cdot (T_m + 273.15) \cdot \ln(I_{\text{sc}}) + \alpha_2 \cdot (T_m + 273.15) + \epsilon \tag{8}$$

where α_i $(i = 0, 1, 2)$ are fitting coefficients, and ϵ is the error term. From (1) and (2), it can be seen that $\alpha_1 = N_c \frac{nk_B}{q}$. With all other parameters in α_1 known, ideality factor n can be obtained from α_1.

Since the temperature coefficient $\alpha_{I_{\text{sc}}}$ is generally negligible (about 0.04%/°C to 0.05%/°C for a commercial crystalline silicon module), I_{sc} and irradiance then have a simple linear relationship

$$I_{\text{sc}}(G_{\text{POA}}) = k \cdot G_{\text{POA}} + \epsilon \tag{9}$$

where k is a fitting coefficient.

The RC I_{sc} value, denoted as $I_{\text{sc}}^{\text{RC}}$, is obtained by fitting a simple linear model as shown in (9), then substitute $G_{\text{POA}} = 1000$ W/m^2 to obtain the predicted value.

As shown in (8), the temperature correction model will be built with I_{sc} and module temperature T_m as independent variables, and the ideality factor n can be calculated from fitting coefficient α_1 of (8). Once the model is built for the selected data analysis period, the reference temperature T_m^{RC} is substituted into (8). Together with the original varying I_{sc} values, the resulting I_{sc} and temperature-corrected V_{oc} pairs make up the *Analytic* I_{sc}–V_{oc} curve. Given long enough time-series I–V data, the temperature-corrected I_{sc}–V_{oc} curves of each analysis period can also form a sparser time series.

With the fitted *Analytic* I_{sc}–V_{oc} curve, a so-called pseudo I–V curve can be obtained following superposition principle, by applying the following equation to every I_{sc} value on the curve, while keeping V_{oc} values the same [23]

$$I_{\text{psd}} = I_{\text{sc}}^{\text{RC}} - I_{\text{sc}} \tag{10}$$

where I_{psd} stands for the current values in the pseudo I–V curve.

C. Correcting I–V Features to RC

Pseudo I–V and real I–V curves of a sample module can be compared to calculate different power loss modes, which will be described in detail in Section II-D. In order to make the pseudo and real I–V curves directly comparable, real I–V curves must be collected at or corrected to the RC. There are different ways to approach this.

First, original time-series data can be filtered to find I–V curves taken when ambient conditions match the RC. However, this vastly limits the range of usable data, and may result in discontinuous time series for modules in Köppen–Geiger (K–G) climate zones where there are few clear-sky days or which have large temperature fluctuations.

Alternatively, there are a few previous studies [24], [25] that have demonstrated linear interpolation or extrapolation of I–V curves, and similar methods has also been defined by IEC 60891 [26] and ASTM E1036 [27].

In our current work, instead of trying to translate the entire I–V curve, several key I–V features will be fitted based on a large-scale real world data, with physics-based equations. All the experimental values of I–V features are extracted by the ddiv package in *R* [9], [10], including I_{sc}, V_{oc}, I_{mp}, V_{mp}, P_{mp}, and R_{s}.

Equations (4) and (5) can also be simplified to the following forms:

$$I_{\text{mp}}(I_{\text{sc}}, T_m) = \beta_0 + \beta_1 \cdot (T_m + 273.15) \cdot I_{\text{sc}} \beta_2 \cdot (T_m + 273.15) \cdot I_{\text{sc}}^2 + \epsilon \tag{11}$$

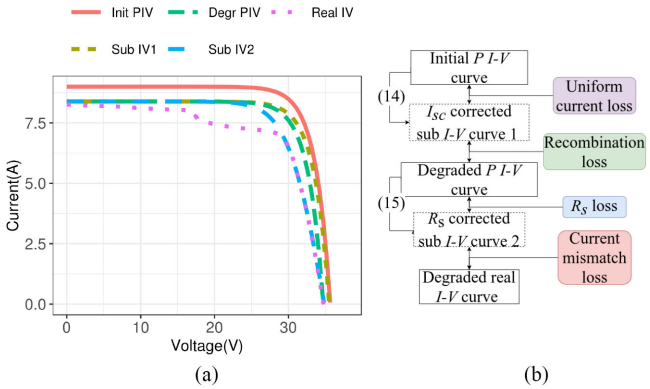

(a) (b)

Fig. 2. Demonstration of power loss calculation. Pseudo I–V curve is abbreviated to PIV. Different loss modes can be calculated from the difference of P_{mp} values between five different curves shown in (a) and (b).

$$V_{\text{mp}}(I_{\text{sc}}, T_m) = \gamma_0 + \gamma_1 \cdot (T_m + 273.15) \cdot \ln(I_{\text{sc}}) + \gamma_2 \cdot \{(T_m + 273.15)\ln(I_{\text{sc}})\}^2 + \gamma_3 \cdot (T_m + 273.15) + \epsilon \quad (12)$$

where β_i $(i = 0, 1, 2)$ and γ_i $(i = 0, 1, 2, 3)$ are fitting coefficients.

From (7), the following equation can be used for modeling:

$$R_s(I_{\text{sc}}, T_m) = \zeta_0 + \zeta_1 \frac{T_m + 273.15}{I_{\text{sc}}} + \epsilon \quad (13)$$

where ζ_0 and ζ_1 are fitting coefficients.

Then, RC T_m^{RC} and $I_{\text{sc}}^{\text{RC}}$ can be substitute into (11)–(13), to obtain predicted I_{mp}, V_{mp}, and R_{s} under the same RC during each analysis period.

D. Power Loss Mechanism Calculation

To perform the mechanistic power loss calculation for each data analysis period, I–V and pseudo I–V curves are corrected to the same RC.

Following the methodology of Guo *et al.* [13] and Walters *et al.* [21], corrections to the pseudo I–V curve of a module can be made to include observed changes in I_{sc}, V_{oc}, and R_{s}. Curves that include above corrections are referred to as sub I–V curves. A simple process flowchart and a set of demonstration curves can be seen in Fig. 2.

The initial pseudo I–V curve from the beginning of data is considered to be the ideal case (or baseline) where no degradation effect is present. Degraded pseudo I–V curves are obtained from each analysis period after the first one, and include uniform current loss and recombination loss.

Sub I–V 1 includes I_{sc} correction from original initial pseudo I–V curve, and can be obtained by applying the following equation to every I_{sc} of the initial pseudo I–V curve:

$$I_{C1} = I_{\text{init}} - \Delta I_{\text{sc}} \quad (14)$$

where ΔI_{sc} is the difference between I_{sc} of initial and degraded pseudo I–V curves, I_{C1} is the I values of sub I–V curve 1, and I_{init} is the I values of initial pseudo I–V curve. The V values remain the same with initial pseudo I–V curve.

Uniform current loss is obtained from the P_{mp} difference of initial P I–V and sub I–V 1, and recombination loss is obtained from the P_{mp} difference of sub I–V 1 and degraded P I–V.

Sub I–V 2 includes R_s correction from the degraded pseudo I–V, and can be obtained by applying the following equation to each V on the curve and keeping I values the same:

$$V_{C2} = V_{\text{degr}PIV} + I \cdot R_{s-\text{degr}PIV} - I \cdot R_{s-IV} \quad (15)$$

where V_{C2} is the V values of sub I–V curve 2. The subscript degrPIV indicates features from degraded pseudo I–V curve, and IV indicates real I–V curve.

R_s loss can obtained from the P_{mp} difference of degraded P I–V and sub I–V 2.

Then finally, the real I–V curve contains all four types of power loss, namely uniform currently loss, recombination loss, R_{s} loss, and current mismatch loss. Current mismatch loss can obtained from the P_{mp} difference of sub I–V 2 and real I–V curve.

An *R* package $SunsV_{\text{oc}}$ has been published to the Comprehensive *R* Archive Network [41], which contains user-friendly functions that can construct outdoor *Analytic* I_{sc}–V_{oc} curves and perform power loss calculations on users' time-series data. With this method, instead of having to correlate power loss with changes in I–V characteristics, all power loss modes are quantified in contribution to module power loss, and are directly comparable. Combined with the time-series I–V dataset, it allows measurement and tracking of power loss due to each degradation mechanism, including uniform current loss, recombination loss, series resistance loss, and current mismatch loss, over the life of the PV module.

TABLE II
DESCRIPTION OF MODULES USED IN CURRENT WORK

Module	Location	Cell type	# of Cells	Age (Mon)	KGC
SunFarm mini	CLE	PERC	4	9	Cfa
Fraunhofer-ISE A	GC	Al-BSF	72	88	BWh
Fraunhofer-ISE B	NEG	Al-BSF	80	59	BSh

KGC stands for K–G climate zone.

III. EXPERIMENTAL METHODS

A. Outdoor I–V Curve Tracing

SDLE Sunfarm: This test facility is located in Cleveland, Ohio (KG Cfa climate zone [28], [29]), and maintained by the SDLE Research Center. Full-size commercial PV modules and 4-cell minimodules are mounted on a fixed rack, and individually controlled and operated by a Daystar multitracer system at their peak power during daylight hours. A Daystar MT5 Multitracer was used to obtain time-series I–V curve data at 10-min intervals, and time-series power, voltage and current collected every minute [30].

The PV module's backsheet temperature is measured by an Omega C01-T thermocouple attached to the backsheet, behind

TABLE III
EVALUATION OF V_{OC}, V_{MP}, R_S, I_{SC}, I_{MP}, AND P_{MP} MODELS OF THREE MODULES

Module	# of intervals	V_{oc} Adj R^2		V_{oc} RMSE		V_{mp} Adj R^2		V_{mp} RMSE		R_s Adj R^2		R_s RMSE	
		Med	Sd	Med	Sd	Med	Sd	Med	Sd	Med	Sd	Med	Sd
SunFarm mini	52	0.99	0.009	0.007	0.016	0.81	0.102	0.03	0.056	0.81	0.213	0.014	0.007
Fraunhofer-ISE A	379	0.98	0.029	0.28	0.095	0.92	0.229	0.47	0.491	0.60	0.308	0.14	0.234
Fraunhofer-ISE B	311	0.98	0.010	0.15	0.041	0.95	0.075	0.28	0.177	0.93	0.215	0.10	0.177
Module	# of intervals	I_{sc} Adj R^2		I_{sc} RMSE		I_{mp} Adj R^2		I_{mp} RMSE		P_{mp} RMSE			
		Med	Sd	Med	Sd	Med	Sd	Med	Sd	Med	Sd		
SunFarm mini	52	0.96	0.181	0.41	0.304	1.00	0.003	0.06	0.058	0.35	0.162		
Fraunhofer-ISE A	379	0.99	0.024	0.17	0.087	1.00	0.093	0.07	0.274	2.01	1.288		
Fraunhofer-ISE B	311	0.99	0.006	0.20	0.090	1.00	0.015	0.05	0.095	1.50	0.761		

Adjusted-R^2 and RMSE are used as evaluation metrics here. Since models were built for each analysis period and each model has different Adj R^2 and RMSE value, median (med), and standard deviation (sd) of each feature over all analysis periods are shown here.

one cell of the 4-cell minimodule, and has the same time interval as the I–V data.

Fraunhofer-ISE: This dataset was provided by Fraunhofer-ISE as part of a research collaboration [31]. It consists of time-series P_{mp} and I–V curve data, acquired from 2 PV modules in 2 different locations and KG climatic zones [32]: 1 in Gran Canaria (BWh climate zone), and 1 in the Negev desert (BSh climate zone). BWh represents a hot desert climate, BSh represents a hot semiarid climate. Above two full-size modules were mounted on fixed racks, module temperature was measured with Pt100 sensors, which are attached behind a centrally located cell on each module.

The time-series data extends for 5–8 years of outdoor exposure time with I–V curves measured every 10 min. The I–V curves were acquired using ESL Solar 500 tracer made by ET Instrument [33]. Table II gives descriptions of the 2 PV modules from this dataset that were analyzed in this article. The massive number of I–V curves (over 2 000 000) allows us to obtain statistically significant results and valuable insights for constructing outdoor I_{sc}–V_{oc} curves. Moreover, the relatively long system age also made time-series analysis on power loss modes possible.

B. Laboratory $Suns$-V_{oc} Measurement

Before the 4-cell minimodule was fielded on SDLE Sunfarm, each individual cell in the minimodule was measured using a Sinton $Suns$-V_{oc} instrument [15], [17], [34]. The temperature of the wafer stage was controlled at 22 °C. Then, given that the cells are connected in series, the lab-based $Suns$-V_{oc} curve of a 4-cell minimodule is obtained by adding the 4 cell-level $Suns$-V_{oc} curves in voltage.

IV. RESULTS

The *Analytic* I_{sc}–V_{oc} method was applied to each data analysis period of three different modules' I–V data. Those three modules varies in size, system age, location, and climate zone. Then, given a sufficiently long time series, the calculated I_{sc}–V_{oc} curves can be combined with the I–V data of the same data analysis period to calculate power loss modes. The information of all three modules analyzed in current work is listed in Table II.

Evaluation metrics including adjusted-R^2 and root mean square error (RMSE) of V_{oc}, V_{mp}, R_{s}, I_{sc}, I_{mp}, and P_{mp} models of three samples are listed in Table III. Since a physics-based model was fitted for each analysis period for every I–V feature listed above, the median and standard deviation of metrics of each feature over all analysis periods are given in the table. One exception here is P_{mp}. Predicted P_{mp} was the product of predicted I_{mp} and predicted V_{mp}, and not directly obtained from a regression model, thus an adjusted-R^2 value is not available, and RMSE is obtained by comparing predicted P_{mp} and measured P_{mp}.

A. Short Term Outdoor Minimodule

In order to prove the accuracy of the outdoor V_{oc} temperature correction, each cell of a 4-cell minimodule was measured with the Sinton $Suns$-V_{oc} instrument, and then the minimodule was mounted on the SDLE SunFarm for I–V curve tracing.

The V_{oc} temperature correction model for this minimodule was built on roughly one month of data. Then, corrected V_{oc} was obtained by substituting 22 °C into the model.

The corrected outdoor I_{sc}–V_{oc} curve shows great agreement with laboratory Sinton result, as shown in Fig. 3. Furthermore, both outdoor and laboratory $Suns$-V_{oc} results overlap with the original I_{sc} and V_{oc} pairs taken around 22 °C.

Six months of continuous time-series I–V curves were obtained for the same minimodule, and with an analysis period of seven days, *Analytic* I_{sc}–V_{oc} and power loss mechanisms were calculated. From Fig. 4, the extracted power loss modes exhibit relatively stable trends, with recombination loss and R_s loss showing slight decreasing trends.

B. Long Term Outdoor Data of Full-Size Modules

Two modules from Fraunhofer-ISE consisting of long, multiyear, continuous I–V data are used for time-series analysis of power loss modes. Mounted in two different KG climate zones, the modules show distinct power loss behavior in Figs. 5 and 6.

For module A in a hot desert climate zone, the uniform current loss, induced by decrease in I_{sc}, shows large, temporary decreases. This behavior, in general, can be caused by snow, soiling, or uniform shading, which can be resolved with cleaning

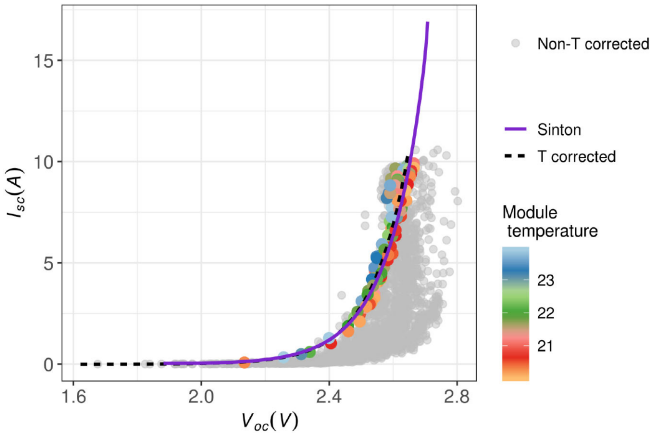

Fig. 3. Outdoor and indoor $Suns$-V_{oc} comparison of 4-cell minimodule. All original experimental data are shown in light gray, and original data taken at 20–24 °C are highlighted with color. V_{oc} on x-axis does not start from 0, to better show data near P_{mp}.

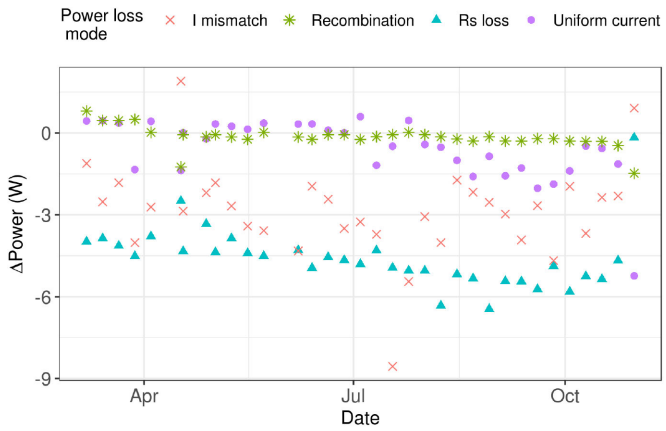

Fig. 4. Half year of calculated power loss modes for a 4-cell PERC minimodule fielded in Cleveland, Ohio.

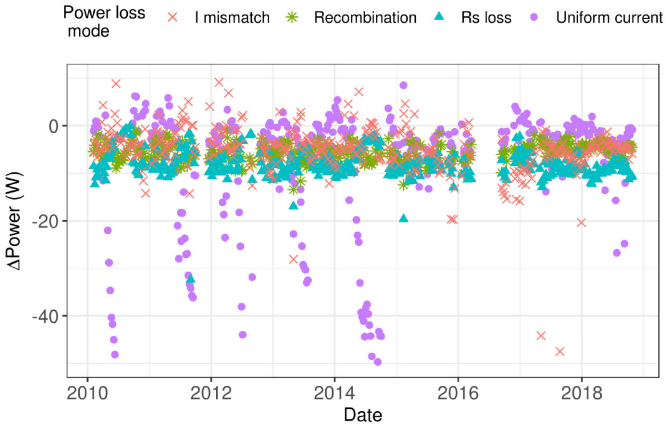

Fig. 5. Time-series power loss modes of Fraunhofer-ISE module A in BWh (hot semiarid climate zone).

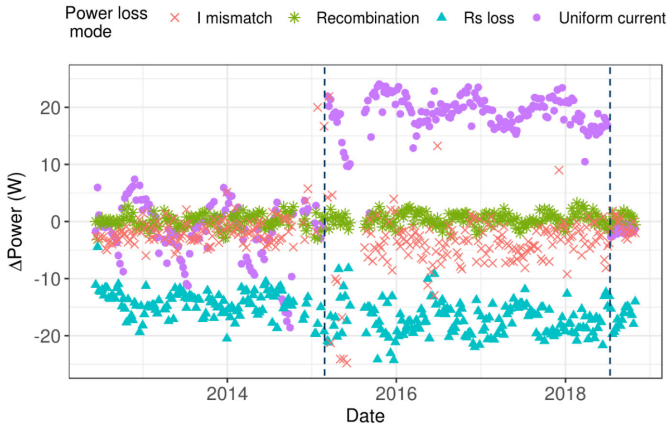

Fig. 6. Time-series power loss modes of Fraunhofer-ISE module B in BSh (hot desert climate zone). Notice that the y-scale is different with previous figure. Two dates where there were sudden changes in I_{sc} are marked with dashed lines.

or clearing off the module. Use module A as an example, no regular cleaning was scheduled before 2015, thus the dust or sand has been accumulating on the module surface and was only cleaned by occasional (and seasonal) rain. Starting from 2015, the module was cleaned every week.

As for the other power loss modes, R_s loss showing a slight decreasing trend over time, indicating that there is corrosion occurring within the module. Recombination loss and current mismatch loss showed stable trends.

As for module B in a hot semiarid climate, while uniform current loss exhibited the most change, the behavior and cause is quite different from the previous module. Marked in Fig. 6, the sudden increase in I_{sc} after year 2015 resulted in a positive uniform current loss, which means that the power (corrected to reference irradiance and temperature) is higher than the baseline value. Another sudden change in I_{sc} can be seen in the middle of 2018, where the uniform current loss experienced a sudden drop.

This peculiar dataset will be discussed in greater detail as a case study in Section V-A, to better illustrate that the *Analytic* I_{sc}–V_{oc} method can not only be used to detect the degradation of PV module, but also abnormalities during the regular operation of a solar power plant.

V. Discussion

A. Applications of Power Loss Modes Calculation

A number of different advanced characterization methods are being developed and applied to evaluate degradation of PV modules in the field, including electroluminescence, photoluminescence, and external quantum efficiency. However, the output of these methods are usually expressed in an abstract way, such as the pixel intensity of an image. It is hard to directly compare degradation features from two different methods, without first correlating them to the decrease in power [35]. By expressing different degradation modes in terms of power loss, with units of watts or % nominal power, the results are clearly quantified and directly comparable. Moreover, if other characterization

methods are available, their results can also be compared with the calculated mechanistic power losses.

1) Real-Time Monitoring: The four degradation modes included in this work come from four different features, namely I_{sc}, V_{oc}, R_{s}, and current mismatch. While V_{oc} and R_{s} generally reflect long-term degradation, I_{sc} and current mismatch can capture both permanent and transient changes.

Uniform current loss is mostly associated with the amount of light reaching the cells, which could be affected by permanent changes like encapsulant discoloration, or temporary conditions such as shading, snow coverage or soiling. Current mismatch loss is associated with the activation of bypass diodes. This can occur due to transient changes like partial shading or poor electrical connection, or permanent changes in the module like cell cracking leading to inactive regions of cells [36].

Thus, when a large power loss is observed for uniform current or current mismatch loss modes, the module can be checked for loose connection, surface soiling, or obstruction to prevent unnecessary loss of power.

2) Long Term Degradation Trends: For loss modes resulting from the slow, permanent degradation, time-series power loss results can be used to calculate the rate of change for each loss mode. While some loss modes cause greater overall power loss than others, i.e., R_{s} loss seen in Fig. 6, the trends (slopes) of loss mode time series indicate their contributions to module degradation. Since all loss modes in this method are directly quantified by the amount of power loss in Watts, dominant degradation modes can be rank-ordered by the slope of their time series trends.

3) Case Study on Fraunhofer-ISE Module B: For Fraunhofer-ISE module B, there are two sudden changes in the power loss modes result calculated from original data, especially uniform current loss (see Fig. 6).

It should be noted that the increase in power does not mean an increase in actual power output, but instead the power at RC (1 sun irradiance and a median module temperature at 1 sun, T_m^{RC}). This means that if the measured G_{POA} is different from actual G_{POA}, there would be mismatch between calculated power at RC and actual power at RC. Sensor drifting will lead to a gradual change with a rate of less than 1% a year [37]. For example, if the sensor is accurate, it would record 1000 W/m^2 under 1 sun. If there was sensor drifting, if it records 950 W/m^2 when the module is producing 1 sun power, P_{mp} at RC would be "overestimated" by a factor of 1000/950. Events such as change of sensor, sensor calibration or change of software settings (calibration coefficient set for an irradiance sensor), would result in a sudden change of recorded irradiance.

Likewise, an inaccurate temperature measurement would also cause a wrong prediction of I–V features.

As for Fraunhofer-ISE module B, two different events happened that both affected measured irradiance. In March 2015, a power outage corrupted the parameter files of the data logger that was recording pyranometer irradiance. And when the data logger was put back on power, either a wrong parameter was inputted, or the value was restored to default. The second change in July 2018 was caused by recalibration of pyranometer, resulting in a slightly higher measured G_{POA} at the same actual G_{POA}.

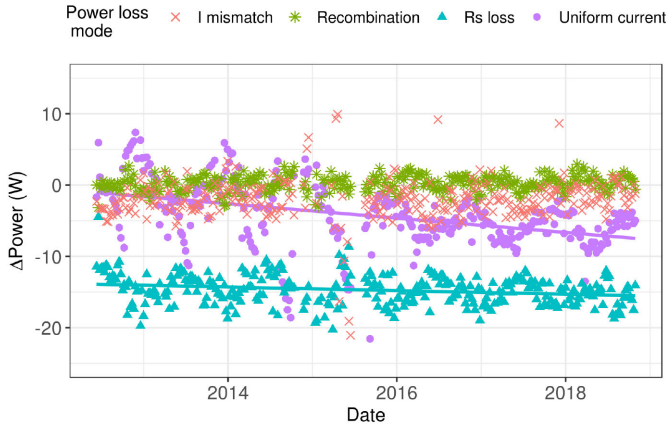

Fig. 7. Power loss modes of Fraunhofer-ISE module B after pyranometer irradiance calibration. Two fitted linear models were added to uniform current loss and R_s loss to better illustrate the change.

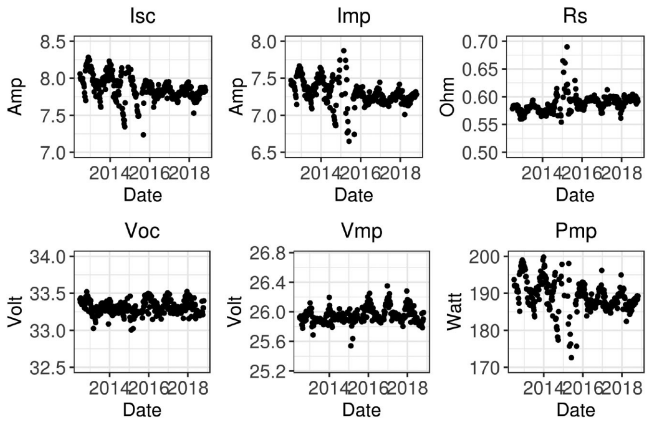

Fig. 8. Fitted parameters at RC (1 sun irradiance, median module temperature around 1 sun, $T_m^{\text{RC}} = 53\,^{\circ}\text{C}$) of Fraunhofer-ISE module B. Each point represents the result of each analysis period.

Above changes were confirmed by recorded operations and management documentation from the power plant.

After recalibrating the pyranometer irradiance, power loss modes of Fraunhofer-ISE module B were recalculated, given in Fig. 7. The most dominant degradation mode, despite the strong seasonality, is uniform current loss. This may be caused by the discoloration of front encapsulant. In addition, similarly with module A, there were seasonal drops in uniform current loss due to severe soiling in the first three years. Only after 2015, the module was cleaned weekly. The second most dominant degradation mode of module B can be identified as R_{s} loss. EVA encapsulant can release acetic acid through Norrish II reaction under strong UV radiation [38], which would cause corrosion.

The predicted I–V features at RC calculated in each data analysis period of module B can be seen in Fig. 8, including I_{sc}, I_{mp}, R_{s}, V_{oc}, V_{mp}, and P_{mp}.

B. Benefits of Data-Driven Modeling Approach

All models used for fitting or temperature correction of I–V features in this work are physics-based models. However, instead

of fixing the physical parameters such as the ideality factor n and temperature coefficient $\beta_{V_{oc}}$, a dynamic data-driven modeling approach was used, where the physical parameters are decided by model coefficients of each data analysis period. There are several reasons for this. First, the physical parameters may not be constant over time, as the overall goal is to quantify the degradation behavior of modules. Second, it would be difficult to determine the values of physical parameters needed in model *a priori*. For example, although most manufacturers provide nameplate temperature coefficients for I_{sc} and V_{oc}, those values usually deviate considerably from the actual temperature coefficients of a specific module. Using the nameplate $\beta_{V_{oc}}$ for temperature correction would result in substantial error, and could not be used for power loss calculation, which requires low uncertainty of pseudo and real I–V curves.

C. Temperature Correction

When correcting either V_{oc} points or I–V curves based on module temperature, it is important to choose a realistic correction temperature for a fielded module. Although the STC of 25 °C, 1000 W/m^2, and air mass 1.5 is relevant for quality control in a factory (as the name indicated, it is a test condition), it is far different from the real-world working conditions for fielded modules in most climatic zones. To avoid extrapolating outside of the experimental data range, we choose a uniform correction temperature that is within the normal operating condition of the module.

In terms of the temperature measurement used in the analysis, there could be several options: cell temperature, module (backsheet) temperature, and ambient temperature. Among these three, although the cell temperature would be the most accurate, as it directly affects V_{oc} and other I–V characteristics in the physical model, it is impossible to measure directly in commercial PV modules. As the second best option, module temperature is relatively easy to obtain by thermocouple, and is considered a decent approximation of cell temperature. There are several methods that can impute cell temperature based on module temperature and other weather data [19], but in order to simplify the modeling process and avoid uncertainties brought by yet another model, module temperature itself is used in various physical temperature correction models detailed in this article. In general, module temperature has a delay of several minutes compared to cell temperature. Since the interval of I–V curve tracing is usually longer than the time delay between cell and module, it is reasonable to use module temperature in the place of cell temperature.

D. Low Irradiance I–V Curves

While other module power degradation rate methods do not require low irradiance I–V curves (and often filter them out before analysis), these datapoints are crucial for constructing the *Analytic* I_{sc}–V_{oc} curve. In the resulting pseudo I–V curve, points that correspond to low irradiance I–V curves comprise the region near I_{sc}.

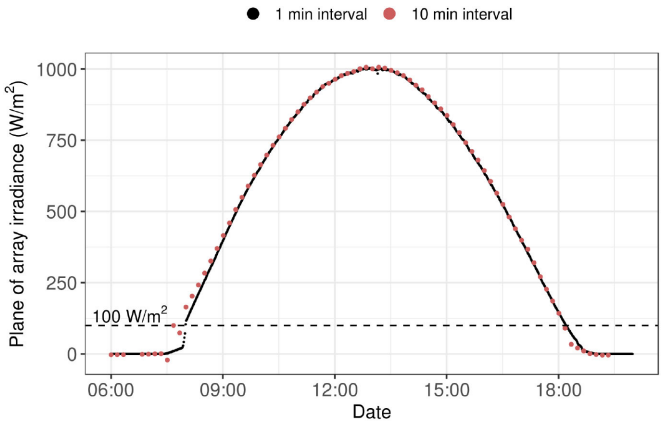

Fig. 9. POA measured with different time intervals in a clear sky day. POA of 100 W/m^2 is marked with dashed line.

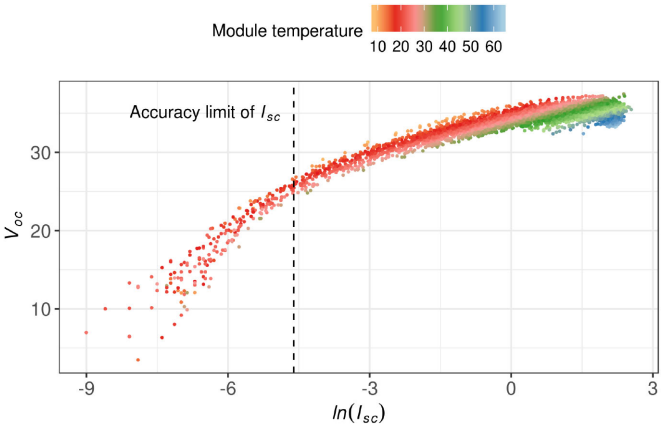

Fig. 10. Three months of I_{sc}–V_{oc} pairs taken by Daystar MT5 multitracer, with an I_{sc} accuracy of 0.01 A. I_{sc} is shown in natural log scale.

As mentioned in Section II, a short measurement interval for I–V curves is ideal to both reduce the data analysis period, and ensure that there are sufficient low irradiance points in the dataset. As an example shown in Fig. 9, in a clear sky day where the irradiance versus time forms a parabolic shape, a 10 min I–V measurement interval results in only 5–6 points below 100 W/m^2 irradiance. Where as when the interval is 1 min, about 80 points with irradiance lower than 100 W/m^2 are collected every day. It should be noticed that although using I–V with short interval is enough to ensure variation in irradiance, variation in module temperature can only be obtained by using longer analysis period. Thus, even though it is possible to construct an *Analytic* I_{sc}–V_{oc} curve every day, the model accuracy may be compromised due to a narrow temperature range.

Meanwhile, it is also necessary to filter out the I–V curves taken at extremely low irradiance with I_{sc} below the accuracy of I–V tracer (see Table I). Below the tracer's accuracy limit, the uncertainty of device will be reflected as highly scattered data points in I_{sc}–V_{oc} plot shown in Fig. 10. From (1), we know that V_{oc} should scale with the natural log of I_{sc}. Fig. 10

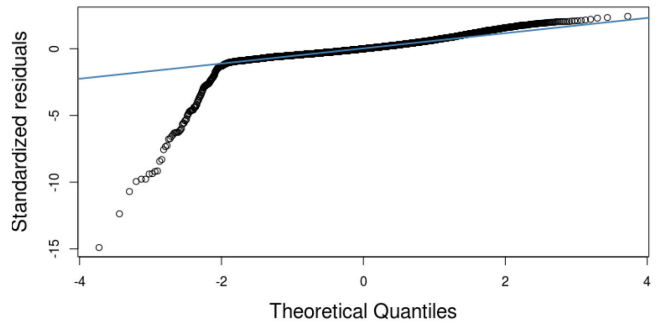

Fig. 11. Normal Q–Q plot for V_{oc} temperature correction model built with a nonfiltered dataset.

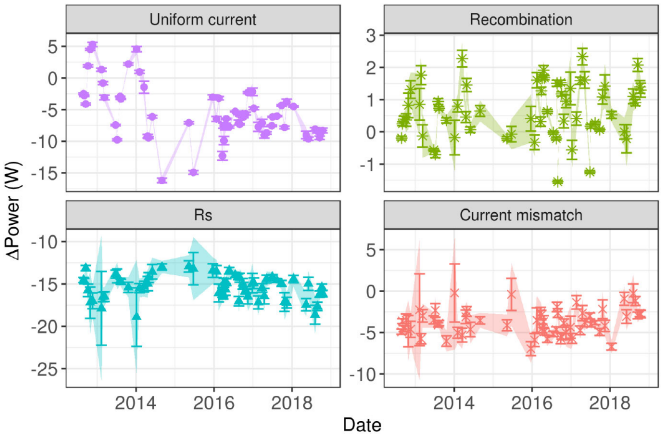

Fig. 12. Uncertainties of power loss modes estimated by the bootstrap method in 60 random analysis periods of Fraunhofer module B. The markers show the mean value of power loss modes out of 1000 bootstrap iterations, error bars show $\pm sd$, and the shaded areas show 95% confidence interval.

demonstrates a change in slope of the V_{oc}-ln(I_{sc}) relationship at the accuracy limit of the tracer. This effect also appears as a heavy tail in standardized residual versus predicted V_{oc} value normal quantile–quantile (Q–Q) plot, shown in Fig. 11.

E. Uncertainty Estimation of Power Loss Modes Using the Bootstrap

The bootstrap method is used to estimate the uncertainty of four power loss modes. The bootstrap is a powerful statistical tool that can be used to quantify the uncertainty of given statistical method whose error is otherwise difficult or impossible to calculate [39], [40].

In the *Analytic* I_{sc}–V_{oc} method, predicted I–V features of each analysis period are used to calculate the corresponding power loss modes of each period. Thus, the uncertainties associated with predicted values propagate in power loss result. Although RMSE of each predicted model listed in Table III can be used in the error propagation calculation, the propagation involves an extremely long chain of different predicted values and could compromise the accuracy of the final error.

Using the bootstrap method, raw observations of I–V curves were resampled with replacement in each analysis period, to generate a bootstrap dataset with the same number of observations. Then, *Analytic* I_{sc}–V_{oc} method was applied on bootstrap dataset to generate power loss results. This procedure was repeated for 1000 iterations on each analysis period. The uncertainty was then determined from the standard deviation as well as 95% confidence interval of 1000 power loss values for each mode in each analysis period.

Sixty analysis periods were sampled from Frauhofer module B to demonstrate the uncertainty of power loss modes calculation, the result is visualized in Fig. 12.

VI. Conclusion

In this article, we presented a robust method – *Analytic* I_{sc}–V_{oc} for building outdoor I_{sc}–V_{oc} curves from time-series I–V fielded commercial PV module data, and analyzing the combined time series to quantify contributions of specific power loss modes.

Validated by indoor laboratory Sinton $Suns$-V_{oc} measurement, outdoor I_{sc}–V_{oc} curves reflect information from all I–V data collected at extensive range of module temperature and irradiance in a given data analysis period, without ever interrupting the regular operation of module. In comparison, outdoor I–V measurements can be biased by environmental conditions, and without a proper I–V translation method, it would be hard to select a representative I–V curve.

In addition, given a long enough time-series I–V datastream, constructed outdoor I_{sc}–V_{oc} curves can also form a time series themselves. This allows for calculation of four different time-series power loss modes: uniform current loss, recombination loss, R_s loss, and current mismatch loss. All loss modes are quantified by the amount of power loss in Watts, making them directly comparable. With that, the dominant degradation mode of a specific module type or climate zone can be quantified.

A full-size Al-BSF module in BSh climate zone (hot semi-arid) was discussed in detail. The dominant power loss mode was found to be uniform current loss, which can result from encapsulant discoloration. Moreover, results of this dataset also revealed several abnormalities during regular operation of the power plant, including a change in pyranometer calibration due to a power outage, and module soiling due to lack of scheduled cleaning.

Acknowledgment

This work made use of the Rider High Performance Computing Resource in the Core Facility for Advanced Research Computing at Case Western Reserve University.

References

[1] International Energy Agency, "World energy outlook," 2019. [Online]. Available: https://www.iea.org/weo/weo2019/secure/data/

[2] R. H. French *et al.*, "Degradation science: Mesoscopic evolution and temporal analytics of photovoltaic energy materials," *Current Opinion Solid State Mater. Sci.*, vol. 19, no. 4, pp. 212–226, Aug. 2015.

[3] D. C. Jordan and S. R. Kurtz, "Photovoltaic degradation rates—An analytical review," *Progress Photovolt., Res. Appl.*, vol. 21, no. 1, pp. 12–29, 2013.

[4] D. C. Jordan and S. R. Kurtz, "The dark horse of evaluating long-term field performance—Data filtering," *IEEE J. Photovolt.*, vol. 4, no. 1, pp. 317–323, Jan. 2014.

[5] E. Hasselbrink *et al.*, "Validation of the pvlife model using 3 million module-years of live site data," in *Proc. IEEE 39th Photovolt. Specialists Conf.*, 2013, pp. 0007–0012.

[6] D. Moser *et al.*, "International collaboration framework for the calculation of performance loss rates: Data quality, benchmarks, and trends," in *Proc. 36th Eur. Photovolt. Solar Energy Conf. Exhib.*, Oct. 2019, pp. 1266–1271.

[7] A. J. Curran *et al.*, "Performance loss rate consistency and uncertainty across multiple methods and filtering criteria," in *Proc. IEEE 46th Photovolt. Specialist Conf.*, Jun. 2019, pp. 1328–1334.

[8] A. J. Curran *et al.*, "Determining the power rate of change of 353 plant inverters time-series data across multiple climate zones, using a month-by-month data science analysis," in *Proc. IEEE 44th Photovolt. Specialist Conf.*, Jun. 2017, pp. 1927–1932.

[9] X. Ma *et al.*, "Data-driven I–V feature extraction for photovoltaic modules," *IEEE J. Photovolt.*, vol. 9, no. 5, pp. 1405–1412, Sep. 2019.

[10] W.-H. Huang *et al.*, "Ddiv: Data driven I–V feature extraction," Sep. 2018. [Online]. Available: https://CRAN.R-project.org/package=ddiv

[11] T. J. Peshek *et al.*, "Insights into metastability of photovoltaic materials at the mesoscale through massive I–V analytics," *J. Vacuum Sci. Technol. B*, vol. 34, no. 5, Sep. 2016, Art. no. 050801.

[12] R. Asadpour, X. Sun, and M. A. Alam, "Electrical signatures of corrosion and solder bond failure in C-SI solar cells and modules," *IEEE J. Photovolt.*, vol. 9, no. 3, pp. 759–767, May 2019.

[13] S. Guo, E. Schneller, J. Walters, K. O. Davis, and W. V. Schoenfeld, "Detecting loss mechanisms of C-SI PV modules *in-situ* I–V measurement," in *Proc. Rel. Photovolt. Cells, Modules, Components, Systems. IX*, Sep. 2016, vol. 9938, Art. no. 99380N.

[14] R. A. Sinton, A. Cuevas, and M. Stuckings, "Quasi-steady-state photoconductance, a new method for solar cell material and device characterization," in *Proc. Conf. Record 25th IEEE Photovolt. Specialists Conf.*, May 1996, pp. 457–460.

[15] R. A. Sinton and A. Cuevas, "Contactless determination of current–voltage characteristics and minority-carrier lifetimes in semiconductors from quasi-steady-state photoconductance data," *Appl. Phys. Lett.*, vol. 69, no. 17, pp. 2510–2512, Oct. 1996.

[16] M. J. Kerr, A. Cuevas, and R. A. Sinton, "Generalized analysis of quasi-steady-state and transient decay open circuit voltage measurements," *J. Appl. Phys.*, vol. 91, no. 1, pp. 399–404, Dec. 2001.

[17] M. K. Forsyth, M. Mahaffey, A. L. Blum, W. A. Dobson, and R. A. Sinton, "Use of the Suns-Voc for diagnosing outdoor arrays and modules," in *Proc. IEEE 40th Photovolt. Specialist Conf.)*, Jun. 2014, pp. 1928–1931.

[18] X. Sun, R. V. K. Chavali, and M. A. Alam, "Real-time monitoring and diagnosis of photovoltaic system degradation only using maximum power point—the Suns-Vmp method," *Progr. Photovoltaics: Res. Appl.*, vol. 27, no. 1, pp. 55–66, 2019.

[19] J. A. Kratochvil, W. E. Boyson, and D. L. King, "Photovoltaic array performance model," Sandia Nat. Lab., Tech. Rep. SAND2004-3535, Aug. 2004. [Online]. Available: https://www.osti.gov/biblio/919131

[20] J.-C. Wang *et al.*, "A novel method for the determination of dynamic resistance for photovoltaic modules," *Energy*, vol. 36, no. 10, pp. 5968–5974, Oct. 2011.

[21] J. Walters, S. Guo, E. Schneller, H. Seigneur, and M. Boyd, "PV module loss analysis using system in-situ monitoring data," in *Proc. IEEE 7th World Conf. Photovoltaic. Energy Convers. (A Joint Conf. 45th IEEE PVSC, 28th PVSEC 34th EU PVSEC)*, Jun. 2018, pp. 2204–2208.

[22] M. Wang *et al.*, "Evaluation of photovoltaic module performance using novel data-driven I-V feature extraction and suns-vocdetermined from outdoor time-series I-V curves," in *Proc. IEEE 7th World Conf. Photovolt. Energy Convers. (A Joint Conf. 45th IEEE PVSC, 28th PVSEC 34th EU PVSEC)*, Jun. 2018, pp. 0778–0783.

[23] R. Sinton *et al.*, "A quasi-steady-state open-circuit voltage method for solar cell characterization," in *Proc. 16th Eur. Photovolt. Solar Energy Conf.*, 2019, vol. 1152, pp. 1–4.

[24] B. Marion, S. Rummel, and A. Anderberg, "Current–Voltage curve translation by bilinear interpolation," *Progress Photovolt.: Res. Appl.*, vol. 12, no. 8, pp. 593–607, 2004.

[25] I. Drouiche and S. Harrouni, "Comparative study between two STC translation methods from different conditions," in *Proc. 8th Int. Conf. Model., Identification Control*, Nov. 2016, pp. 258–262.

[26] "Photovoltaic Devices - Procedure for Temperature and Irradiance Corrections to Measured I-V Characteristics, IEC 60891," 2009. [Online]. Available: https://webstore.iec.ch/publication/3821

[27] E44 Committee, "ASTM-E1036 test methods for electrical performance of nonconcentrator terrestrial photovoltaic modules and arrays using reference cells," , ASTM International, Tech. Rep. ASTM-E1036, 2019. [Online]. Available: http://www.astm.org/cgi-bin/resolver.cgi?E1036-15R19

[28] F. Rubel and M. Kottek, "Observed and projected climate shifts 1901-2100 depicted by world maps of the Koppen-Geiger climate classification," *Meteorologische Zeitschrift*, vol. 19, no. 2, pp. 135–141, Apr. 2010.

[29] C. Bryant, N. R. Wheeler, F. Rubel, and R. H. French, "KGC: Koeppen-Geiger climatic zones," Nov. 2017. [Online]. Available: https://cran.r-project.org/web/packages/kgc/index.html

[30] Daystar, Inc., "Daystar MT5 multi-tracer," 2012. [Online]. Available: http://www.daystarpv.com/multitracer3.html

[31] J. Liu *et al.*, "Real-world PV module degradation across climate zones determined from suns-voc, loss factors and I–V steps analysis of eight years of I–V, pmp time-series datastreams," in *Proc. IEEE 46th Photovolt. Specialists Conf.*, Jun. 2019, pp. 0680–0686.

[32] W. Köppen, "The thermal zones of the Earth according to the duration of hot, moderate and cold periods and to the impact of heat on the organic world," *Meteorologische Zeitschrift*, vol. 20, no. 3, pp. 351–360, Jun. 2011.

[33] ET Instrumente GmbH, "Electronic Load ESL-Solar 500," 2018. [Online]. Available: https://et-instrumente.de/images/PDF/2018Englisch/KAT-2018-Electronic20Loads20ESL-Solar-P22-P25.pdf

[34] R. A. Sinton, "SUNS-VOC," 2019. [Online]. Available: https://www.sintoninstruments.com/products/suns-voc/

[35] A. M. Karimi *et al.*, "Generalized and mechanistic PV module performance prediction from computer vision and machine learning on electroluminescence images," *IEEE J. Photovolt.*, vol. 10, no. 3, pp. 878–887, May 2020.

[36] M. Köntges, I. Kunze, S. Kajari-Schröder, X. Breitenmoser, and B. Bjørneklett, "The risk of power loss in crystalline silicon based photovoltaic modules due to micro-cracks," *Solar Energy Mater. Solar Cells*, vol. 95, no. 4, pp. 1131–1137, Apr. 2011.

[37] A. J. Curran, "Lifetime performance modeling of commercial photovoltaic power plants," Ph.D. dissertation, Case Western Reserve Univ., 2019. [Online]. Available: http://rave.ohiolink.edu/etdc/view?acc_num=case1564763825566542

[38] J. Jin, S. Chen, and J. Zhang, "UV aging behaviour of ethylene-vinyl acetate copolymers (EVA) with different vinyl acetate contents," vol. 95, no. 5, pp. 725–732. [Online]. Available: http://www.sciencedirect.com/science/article/pii/S0141391010000911

[39] G. James, D. Witten, T. Hastie, and R. Tibshirani, *An Introduction to Statistical Learning: With Applications in R*, vol. 112. Berlin, Germany: Springer-Verlag, 2013, pp. 187–190. [Online]. Available: https://www.springer.com/gp/book/9781461471370

[40] C. Z. Mooney, R. D. Duval, and R. Duval, *Quantitative Applications in the Social Sciences, No.95. Bootstrapping: A Nonparametric Approach to Statistical Inference*. Thousand Oaks, CA, USA: Sage Publications, 1993, pp. 30–33, doi: 10.4135/9781412983532.

[41] M. Wang *et al.*, "SunsVoc: Constructing Suns-Voc from Outdoor Time-series I-V Curves," May 2020. [Online]. Available: https://CRAN.R-project.org/package=SunsVoc